metals

MDPI

Supplementary Materials

Inverse Design of Aluminium Alloys Using Genetic Algorithm: A Class-Based Workflow

Ninad Bhat [1,*], Amanda S. Barnard [2] and Nick Birbilis [1,3,*]

[1] School of Engineering, College of Engineering, Computing & Cybernetics, The Australian National University, Canberra, ACT 2601, Australia
[2] School of Computing, College of Engineering, Computing & Cybernetics, The Australian National University, Canberra, ACT 2601, Australia
[3] Faculty of Science, Engineering and the Built Environment, Deakin University, Melbourne, VIC 3216, Australia
* Correspondence: ninad.bhat@anu.edu.au (N.B.); nick.birbilis@deakin.edu.au (N.B.)

This document presents the supporting tables for the main text. Figure S1 presents the learning curve for each regressor. Figure S2 shows the mean absolute error of the optimised regressors for each target.

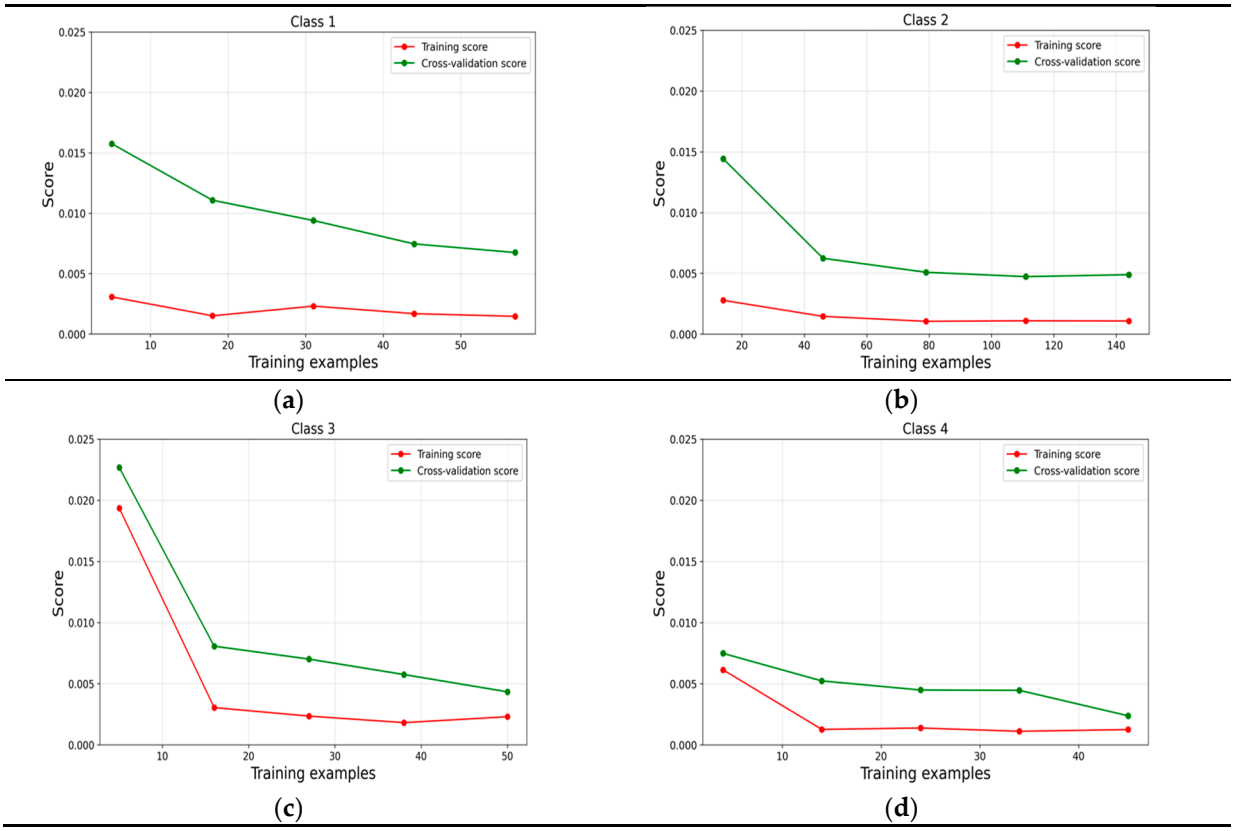

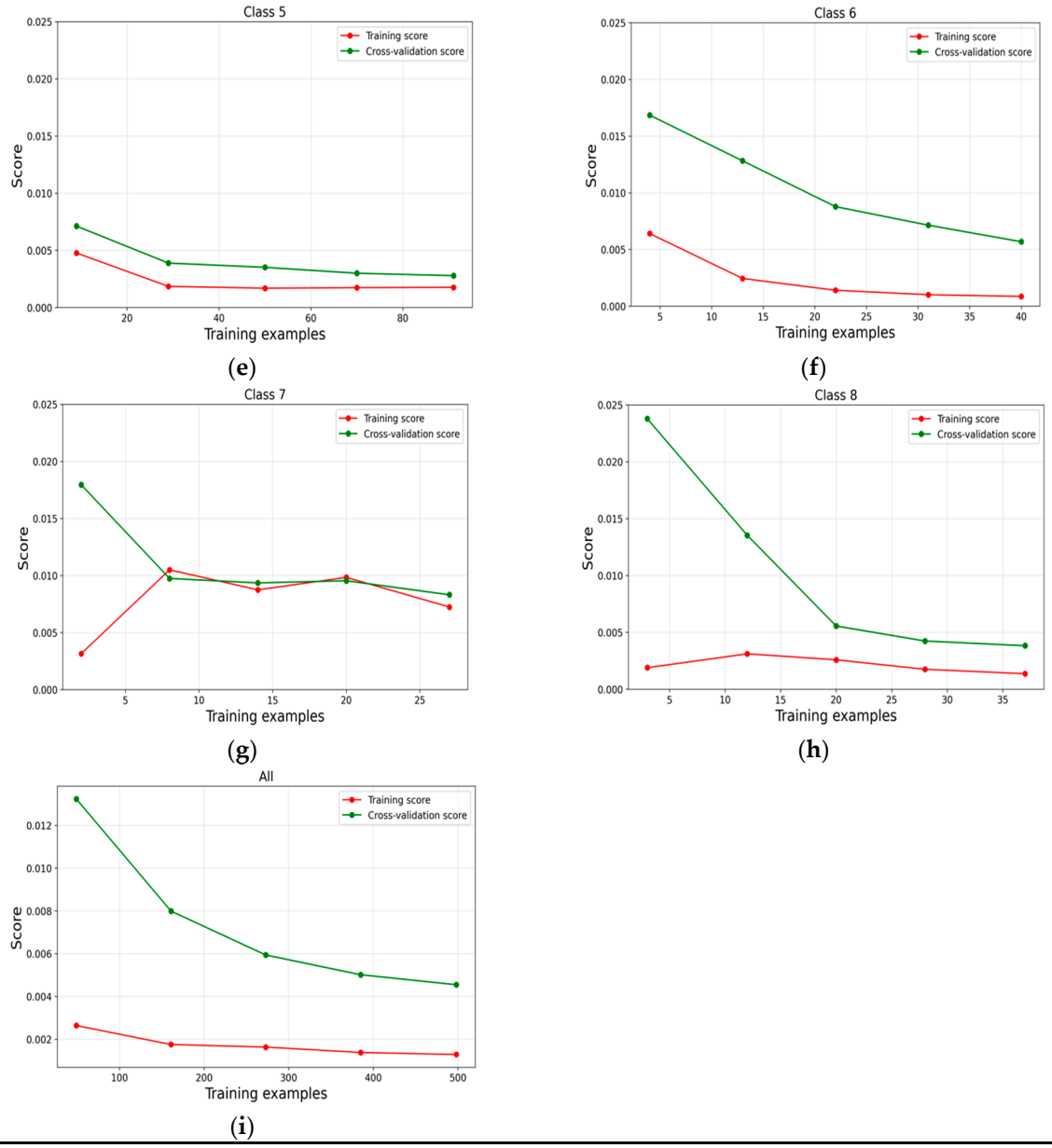

Figure S1. Learning curves for the random forest regressor predicting three mechanical properties. (**a**) R_1, (**b**) R_2, (**c**) R_3, (**d**) R_4, (**e**) R_5, (**f**) R_6, (**g**) R_7, (**h**) R_8, and (**i**) R_all.

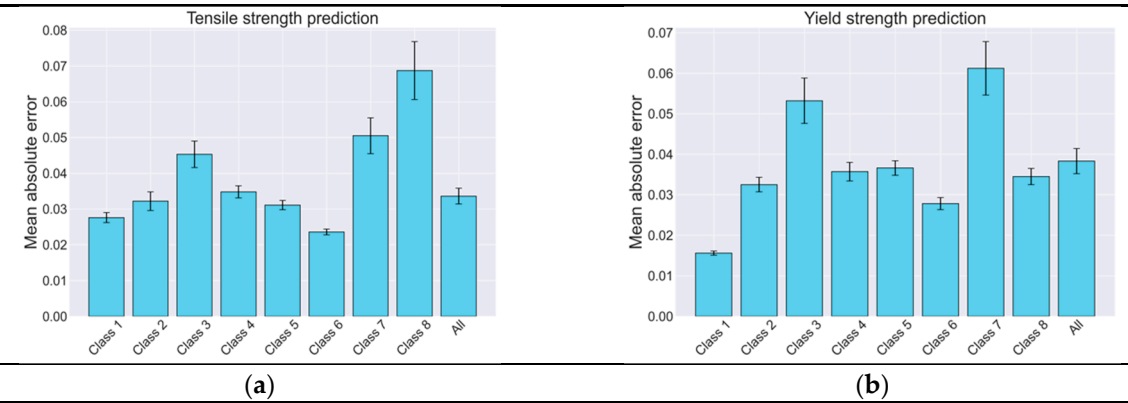

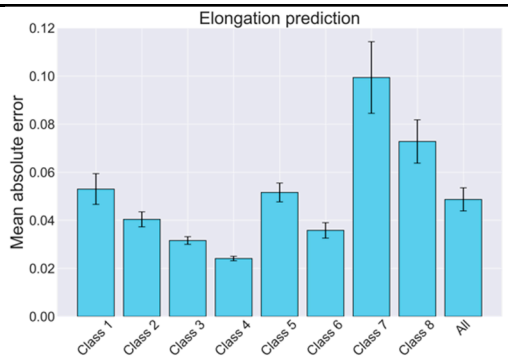

(**c**)

Figure S2. Mean absolute error of prediction of each target for optimised models. (**a**) Tensile strength, (**b**) yield strength, and (**c**) elongation.

Figure S3 illustrates the Pareto front train using each class-based regressor and regressor trained on the entire dataset. Figure S4 depicts the hypervolume over the number of generations, indicating the convergence of the NSGA-II algorithm. Figure S5, Figure S6, and Figure S7 display the predicted concentrations of elements, which are not included in the main text, for $\mathcal{P}_1$, $\mathcal{P}_2$, and $\mathcal{P}_6$, respectively.

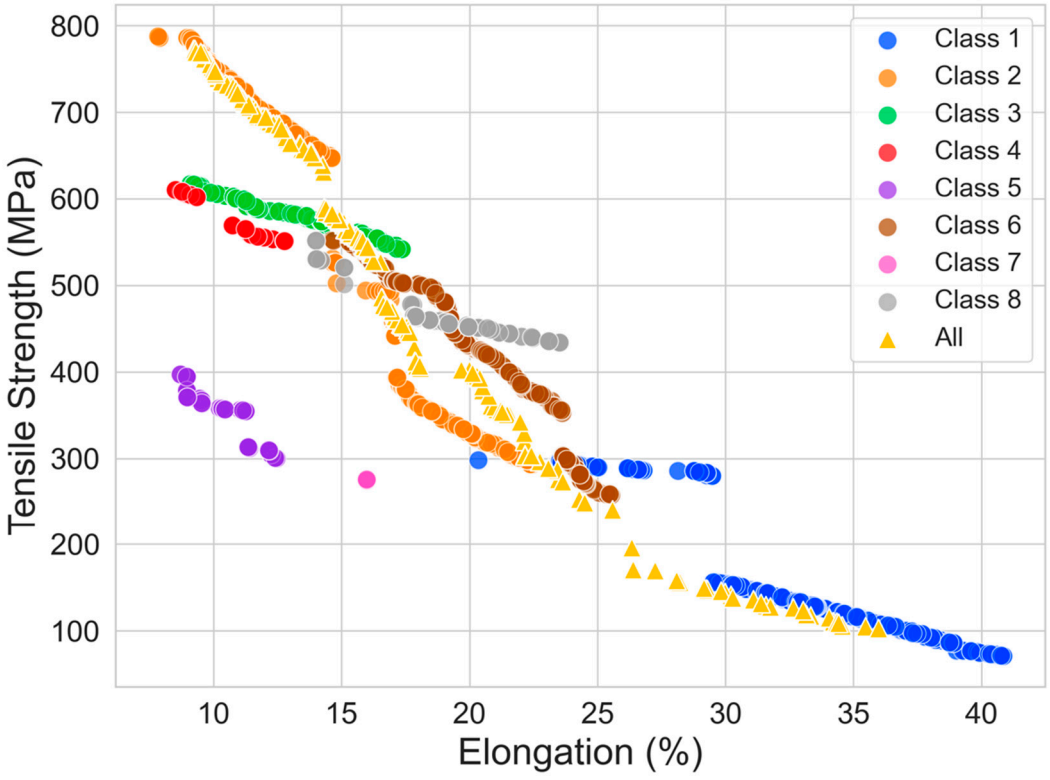

Figure S3. Pareto front for individual classes optimising for tensile strength and elongation.

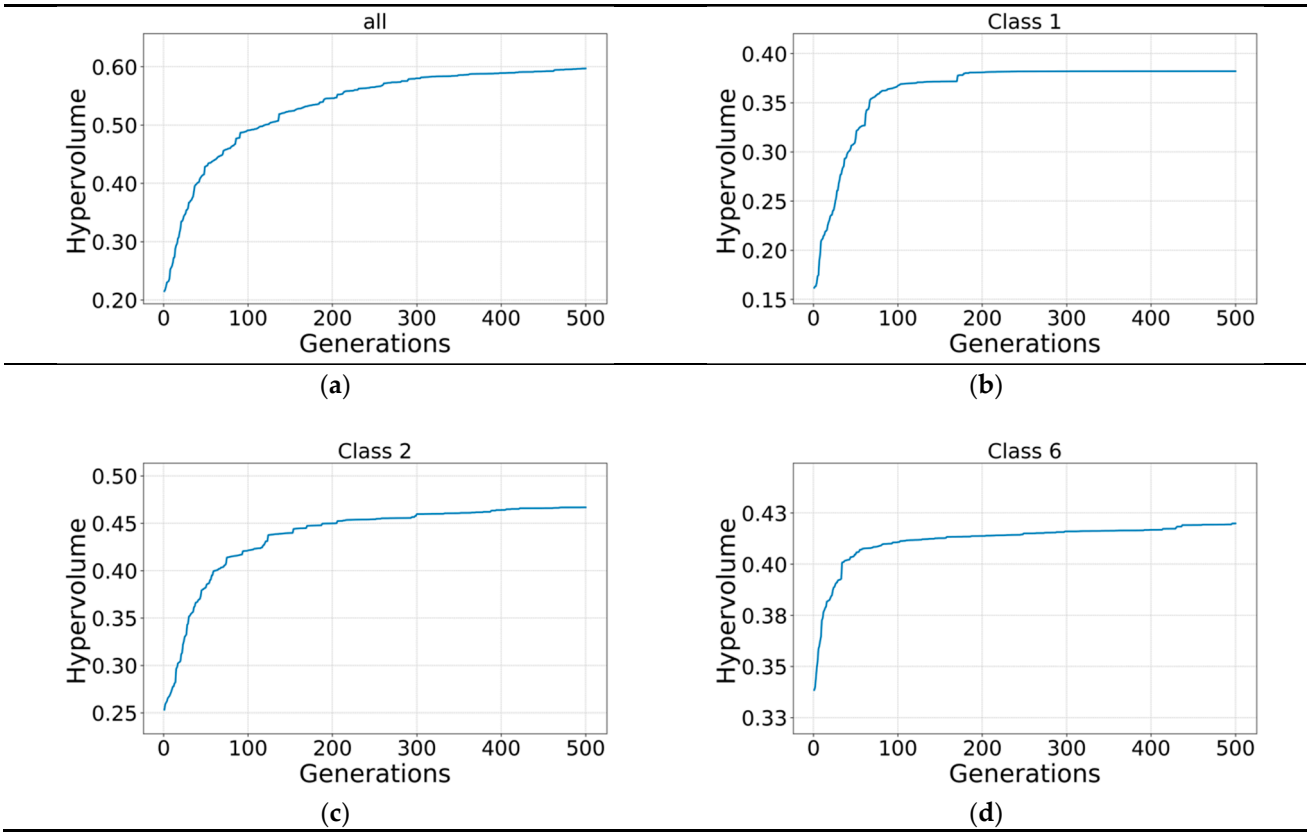

Figure S4. Hypervolume plot showing the convergence of NSGA-II algorithm for (**a**) all, (**b**) Class 1, (**c**) Class 2, and (**d**) Class 6.

Figure S5. Predicted alloy concentrations on Pareto front 1. (**a**) Si concentration, (**b**) Cu concentration, (**c**) Fe concentration, (**d**) Zn concentration, and (**e**) Zr concentration.

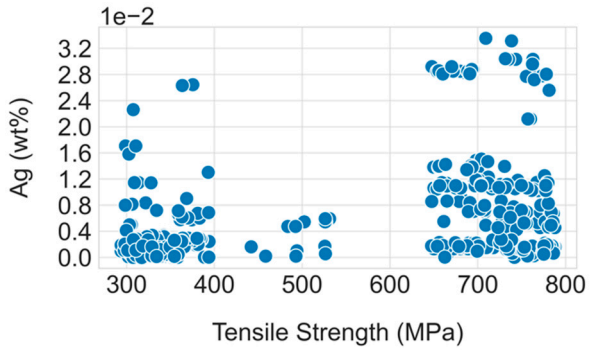
1e−2
Ag (wt%)
Tensile Strength (MPa)

(**a**)

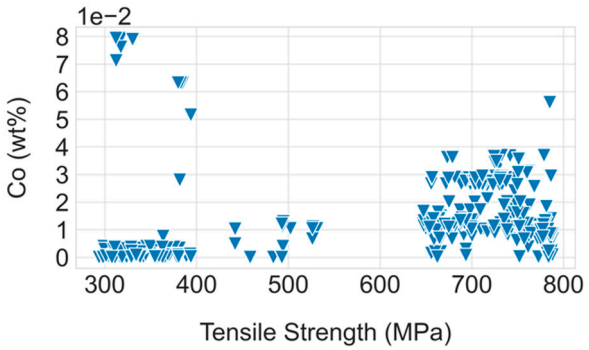
1e−2
Co (wt%)
Tensile Strength (MPa)

(**b**)

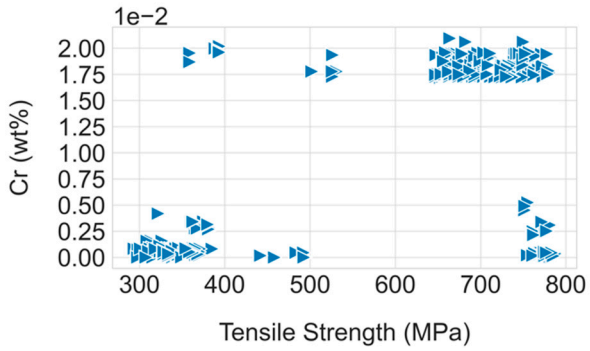
1e−2
Cr (wt%)
Tensile Strength (MPa)

(**c**)

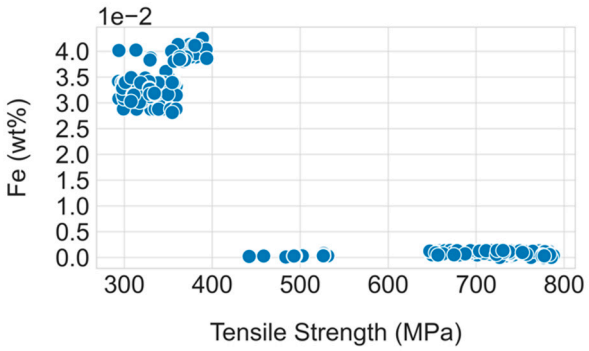
1e−2
Fe (wt%)
Tensile Strength (MPa)

(**d**)

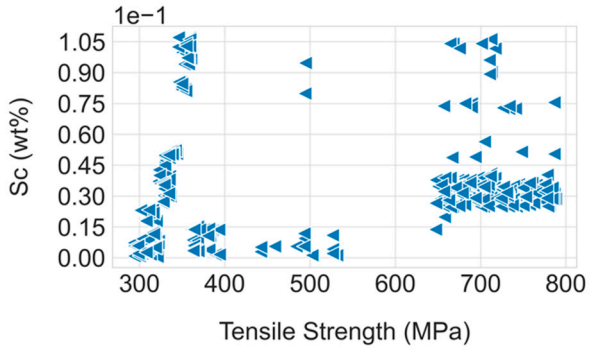
1e−1
Sc (wt%)
Tensile Strength (MPa)

(**e**)

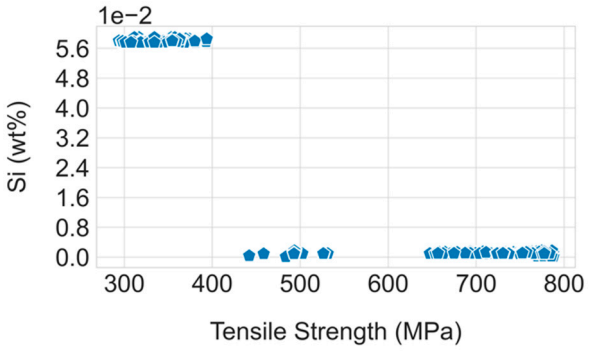
1e−2
Si (wt%)
Tensile Strength (MPa)

(**f**)

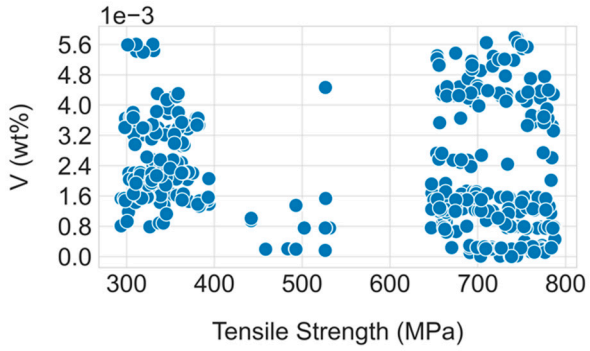
1e−3
V (wt%)
Tensile Strength (MPa)

(**g**)

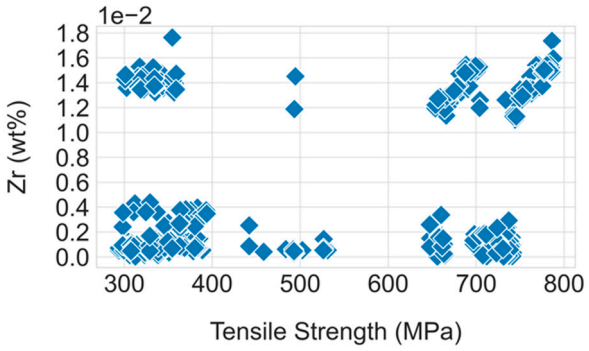
1e−2
Zr (wt%)
Tensile Strength (MPa)

(**h**)

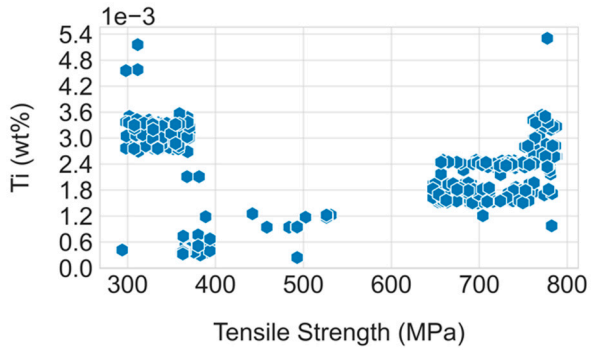

(**i**)

Figure S6. Predicted alloy concentrations on Pareto front 2. (**a**) Ag concentration, (**b**) Co concentration, (**c**) Cr concentration, (**d**) Fe concentration, (**e**) Sc concentration, (**f**) Si Concentration, (**g**) V concentration, (**h**) Zr concentration, and (**i**) Ti concentration.

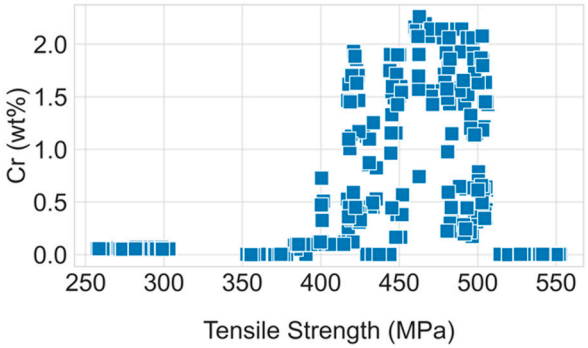

(**a**)

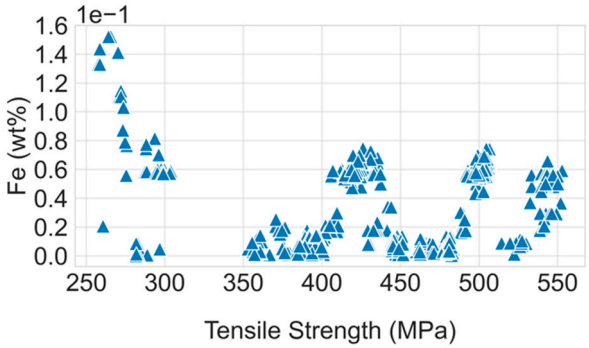

(**b**)

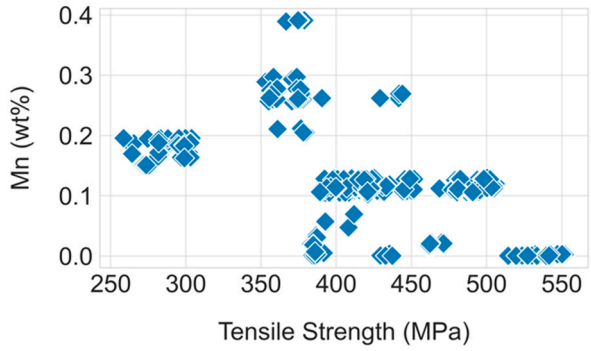

(**c**)

Figure S7. Predicted alloy concentrations on Pareto front 6. (**a**) Cr concentration, (**b**) Fe concentration, and (**c**) Mn concentration.

Figure S8 presents the elbow plot using KMeans clustering for Class 1. The figure suggests that no additional subclusters are present in Class 1.

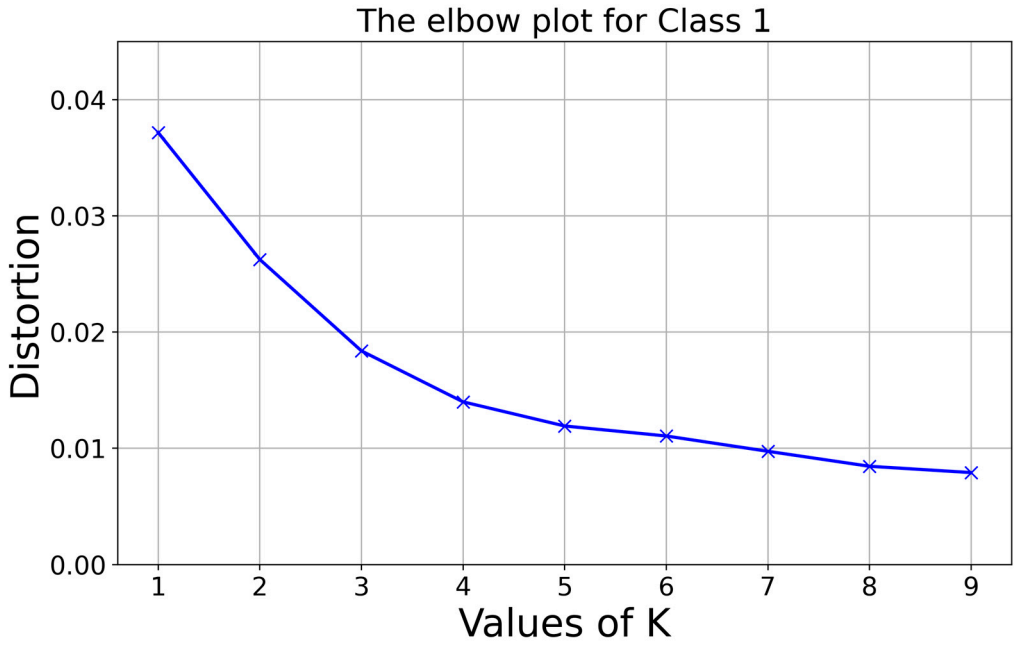

t

Figure S8. Elbow method analysis for the optimal K value in Class 1.